Queensland University of Technology
Brisbane Australia

This may be the author's version of a work that was submitted/accepted for publication in the following source:

Influence of surface hydrophobicity/hydrophilicity of biochar on the removal of emerging contaminants

Adam M. Clurman[1,2], Oscar M. Rodríguez-Narvaez[3], Ayomi Jayarathne[4], Gehan De Silva[5] Mahinda I. Ranasinghe[5], Ashantha Goonetilleke[4], Erick R. Bandala[1*]

[1]Division of Hydrologic Sciences. Desert Research Institute. 755 E. Flamingo Road, Las Vegas, Nevada 89119-7363, USA. E-mail: erick.bandala@dri.edu, Tel: 702 862 5395.
[2]School of Liberal Arts and Science, Nevada State College, 1300 Nevada State Dr, Henderson, Nevada 89002.
[3]Departamento de Química, DCNE, Universidad de Guanajuato, Cerro de la Venada s/n, Pueblito de Rocha, Guanajuato, México, C.P. 36040.
[4]School of Civil and Environmental Engineering, Queensland University of Technology, GPO Box 2434, Brisbane, 4001, Queensland, Australia.
[5]Department of Chemistry. New Mexico Institute of Mining and Technology, 801 Leroy Place, 115 Lopez Chemistry Hall, Socorro, NM 87801.

*Corresponding author: erick.bandala@dri.edu (Erick R. Bandala)

Highlights

- Role of biochar hydrophilicity in the removal of emerging contaminants investigated

- Changes to thermally treated biochar surfaces increased adsorption performance

- Thermal treatment resulted in changes to biochar surface and crystalline structure

- Rate-limiting steps in removal process were adsorbate monolayer and chemisorption

- Anions in aqueous solution exert significant influence on the adsorption process

Graphical abstract
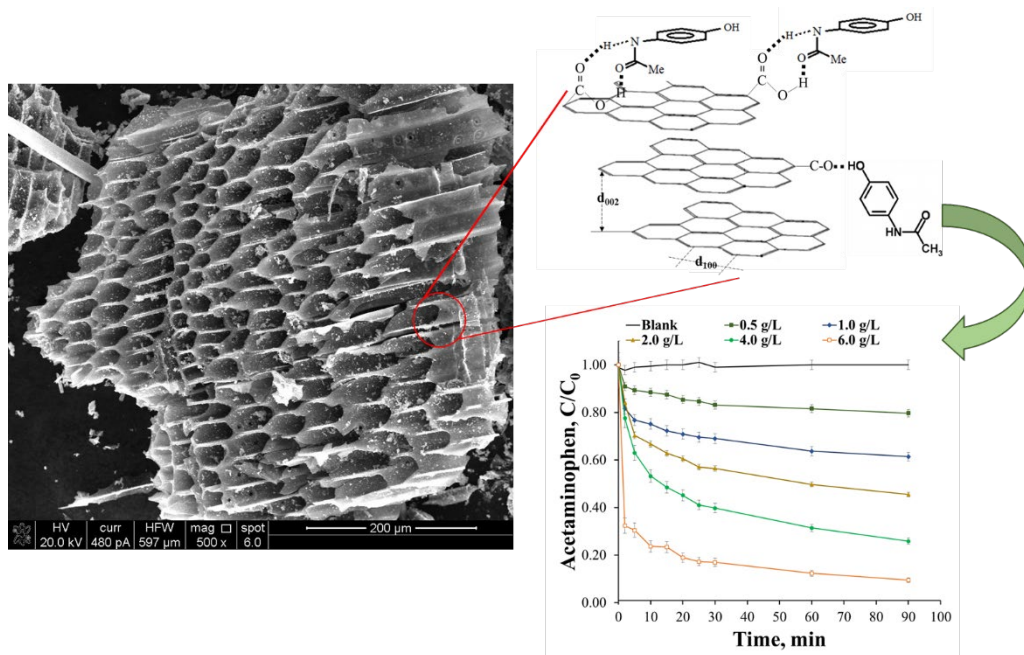
ABSTRACT. This study investigated the removal of Acetaminophen (ACT) using biochars having different physicochemical characteristics. Biochars subjected to post-pyrolysis heat-treatment at 300°C for different treatment times (0, 3.5, 8 and 24 h) were used. The resulting biochars were characterized using FTIR and X-ray diffraction spectroscopy. Experiments for ACT adsorption with different biochars loads (0.0, 0.05, 1, and 2 g L^{-1}) were performed. Using the best performing material, ACT adsorption was investigated for additional biochar loads (4.0, and 6.0 g L^{-1}) and experiments to test the effect of ionic strength were undertaken for different ions (chloride, carbonate, and nitrate) at three different concentrations (0.0, 1.0, 5.0 mM). The results showed that the changes to the surface of the thermally treated biochars increased the adsorption of ACT. The changes in the amount of oxygen-containing functional groups on the surface of the modified biochars (e.g., C=O from 47.8 a.u. to 152 a.u. in the untreated and thermally treated biochars, respectively), as well as modifications to their crystalline structure are considered to be the reason for the observed improvement. Adsorption isotherms and kinetic models suggest the generation of an adsorbate monolayer and chemisorption as the rate-limiting step. The different anions tested were found to have a significant influence on ACT adsorption, related to their electronegativity and steric effect, as confirmed by the multivariate analysis.

Keywords: Biochar, adsorption, drinking water, emerging contaminants, acetaminophen.

1. Introduction

Presence of emerging contaminants (ECs), particularly pharmaceuticals, in aquatic environments has become a significant source of concern because of their potential adverse human and ecosystem health impacts, even at trace concentration levels [1]. Among the different ECs, acetaminophen (ACT) has attracted attention because of its frequent occurrence in aquatic environments related to its increased global production and consumption, mainly in developing countries, uncontrolled disposal of expired medicine and the discharge of poorly metabolized active principle to receiving water bodies [2,3]. According to past epidemiologic and ecotoxicologic studies, ACT is mostly metabolized into N-acetylbenzoquinoneimine (NAPQI), a toxic, active oxidant and electrophilic metabolic intermediate [4]. When excessive dosages of ACT are absorbed, NAPQI bioaccumulates and starts exerting toxic effects on organism, including oxidative stress, generating changes in the thiol groups in cellular proteins, leading to DNA and RNA damage, and oxidation of the membrane lipids [5,6]. This highlights the need for novel, cost-effective treatment processes capable of removing ACT from water environments.

Carbon-based materials have been shown to be not only effective adsorbents, and the solid matrix support transition metal ions and oxides, but also acts as an environmentally friendly catalyst [7–10]. However, the most commonly used carbon-based materials such as carbon nanotubes and graphene have also been reported capable of posing human health and environmental risks when released into the environment [11–15]. Furthermore, the search for carbon-based materials with "green" capabilities which are capable of meeting environmental applications and at the same time do not present potential adverse human health and/or environmental impacts remains an ongoing scientific challenge [16]. In this context biochar could be considered as a suitable material. Biochar is a highly porous carbon-based material produced from feedstock biomass under low-oxygen conditions, which has been reported showing versatile adsorption capability depending on the feedstock used for production [17–19]. The high ability to modify the physicochemical properties

of biochar based on specific needs has resulted in wide application for the removal of a diversity of environmental contaminants [2]. Despite the significant opportunities provided by the ability to custom-modify the properties of biochar, to the best of our knowledge, relatively few studies are available on the benefits of this ability in relation to the removal of ECs, as well as the mechanisms involved or the influence of water quality parameters on the removal of ECs in water. The aim of this study was to assess the effect of increased hydrophobicity/hydrophilicity of the biochar surface on its ability for the adsorption of emerging contaminants in the aqueous phase. This also entailed the identification of the changes in the surface functional groups involved in the adsorption process, as well as the potential mechanisms involved, and the assessment of the effect of ionic strength on the feasibility of engineered biochar application for the adsorption of ACT in aqueous phase, as a case study.

2. Materials and methods

2.1 Biochar preparation

The raw biochar (BC) used in the study was obtained from Biochar Now (Berthoud, USA) produced from beetle-kill pine timber from Colorado at pyrolysis temperature 600 ± 50 °C under limited oxygen for 8 h [10]. The particle size of the untreated biochar was in the range of 0.3-0.7 mm. The BC material has high hydrophobicity (contact angle value >90°, rated as highly hydrophobic) as reported elsewhere [10]. The previous study also found that treating BC at 300°C for different time periods generated significant changes in its hydrophilicity by changing the contact angle from >90° to 69° (considered hydrophilic) [10]. In order to compare the effect of hydrophilicity/hydrophobicity of biochar, other biochars, 3.5BC, 8BC and 24BC, were produced by heating BC to 300 °C in ambient air using a Thermo Fisher Scientific F48025 muffle furnace for different periods of time (3.5, 8, and 24 h, respectively). The different materials (3.5BC, 8 BC, and 24BC) were separated from the ashes produced (about 5%) by screening, using mesh 50 (approx. 0.297 mm particle size) and used in the experiments without further purification. The selection of the heat treatment conditions adopted to produce the hydrophilic biochar material was based on extensive investigations undertaken by Mortazavian et al. [10] where significant changes in the surface characteristics were identified to be influenced by thermal treatment temperature and time duration of the treatment.

2.2 Thermally-treated biochar characterization

The crystallographic study of the different biochar materials produced was carried out using a Panalytical X'Pert PRO powder diffractometer at a scanning rate of 13°/min in the range 2θ of 5-70° with Cu-Kα radiation 45 kV and 40 mA at room temperature. Specific surface functional groups on the different biochars (C=O and C−O) were investigated using a Fourier transform infrared spectroscopy (FTIR, Shimadzu IR Prestige-21 FTIR Spectrophotometer, SHIMADZU Corporation, Japan). For the FTIR analysis, consistent with the method used by our research group in the past [20], the biochars were ground and mixed with potassium bromide (KBr) with a 1/500 mass ratio in order to make pressed pellets. The spectra were recorded in the wave number range of 400–4000 cm^{-1} at a resolution of 4.0 cm^{-1}. Biochar samples were analyzed for C=O and C-O bonds using FTIR spectroscopy. The availability of C=O and C-O bonds was qualitatively and quantitatively analyzed by the peak positions and by calculating the area under the relevant peaks. For quantification of C=O bonds, area under the curves of peaks in the range of 1640-1820 cm^{-1}

was determined and for C-O bonds, the same technique was repeated on the peak appearing around ~1060 cm^{-1}.

2.3 ACT adsorption experiments

ACT adsorption experiments consisted of four different loads (0.0, 0.5, 1.0, and 2.0 g L^{-1}) of the different thermally treated biochar (e.g., BC, 3.5BC, 8BC, and 24BC). All the experiments were performed in duplicate using 0.66 mM (100 mg L^{-1}) ACT solution. Samples (1.0 mL) were taken at different process times (0, 10, 20, 30, 40, 50, 60 minutes and 24 hours) and analyzed for ACT concentration using high-performance liquid chromatography (HPLC). Additionally, for ACT adsorption using 8BC, two larger biochar loads (4 and 6 g L^{-1}) were tested. The effect of ionic strength on the adsorption process was also tested for the best ACT adsorption conditions (8BC, 6 g L^{-1}) using three different concentrations of nitrate, chlorite and carbonate (0.0, 1.0 and 5.0 mM). The effect of the combination of ions was tested using 1 mM concentration of every ion in solution singly, combination of two ions and all the ions simultaneously.

2.4 ACT quantification

For the quantification of ACT in aqueous phase, an Agilent 1200 HPLC system equipped with a reversed-phase Phenomenex Gemini C-18 (5 μm, 4.6 mm× 150 mm) column and UV detector (λ = 260 nm) was used. The mobile phase consisted of a mixture of 70% and 30% (v/v), acetonitrile/trimethylamine (3 mM, pH 6.2) and a flow rate 0.6 mL min^{-1}. The separation was performed at 40°C.

2.5 Multivariate analysis

Two multivariate statistical analysis methods; Hierarchical Cluster Analysis (HCA) and Preference Ranking Organization Method for Enrichment Evaluations (PROMETHEE) together with Graphical Analysis for Interactive Assistance (GAIA) methods were used to identify the relative adsorption performance of untreated and thermally treated biochar with different characteristics, and to rank these according to their adsorption performance. Multivariate analysis allows the investigation of multidimensional data by considering several variables, and can examine complex chemical phenomena and data patterns more accurately and in-depth when compared to univariate/bivariate methods. Further, the analytical outcomes derived from the multivariate analysis methods employed would not have been possible if only univariate/bivariate methods were used. Accordingly, the observations and conclusions derived from this study are further supported by the analysis using multivariate models.

HCA is a multivariate classification method that groups objects (i.e. thermally treated BC) with similar characteristics into clusters [21]. In HCA, the number of clusters is reduced by joining the two closest clusters, resulting in a hierarchy of partitions. The relationships in similarity among clusters can be represented using either a distance matrix or a tree-like branching diagram, termed a dendrogram [22,23]. In a dendrogram, the height of the branch points (i.e. correlation distance) indicates how similar or different these are from each other, such that, the greater the height, the greater the difference. Different linkage methods such as single linkage, average linkage, complete linkage and Ward's method are used to calculate the cluster dissimilarity depending on the data availability. In this study, Ward's linkage method was used to compute the similarity between each object, ensuring that there were no missing data. Minitab 17 software was used for the cluster analysis.

PROMETHEE is a non-parametric data analysis method that evaluates several possible decisions according to different and often conflicting criteria in order to identify the best possible decision whilst ranking them from the best to the worst [24]. PROMETHEE facilitates decision-makers to select the most preferred action (i.e. objects) according to the weight of the corresponding criteria (i.e. variables) using a preference function [25]. Based on the weight and preference function, actions are ranked by calculating the net outranking flow values (ϕ, Phi values). GAIA represents the graphical description of the PROMETHEE ranking. In a GAIA biplot, actions and criteria are represented by points and vectors, respectively. The orthogonal vectors represent the independent variables, whist vectors having acute angles are correlated to each other. The decision axis in GAIA biplot represents the decision power of the method, where the most influential and favorable actions and criteria are located closer to the decision axis. Further details on PROMETHEE analysis can be found elsewhere [25]. In this study, Visual PROMETHEE software was used for the ranking and GAIA analysis.

3. Results and discussion

3.1 Non-treated and thermally-treated biochar characterization

Thermally treated biochar after pyrolysis under atmospheric conditions has been found to change from being highly hydrophobic to hydrophilic depending on the heat-treatment time [10]. This change is considered to be related to the change in the amount of oxygen containing functional groups on the surface of the adsorbent [26,27]. The absorbance bands corresponding to C=O and C–O for the different post-pyrolysis thermally treated biochars found by FTIR analysis are shown in Figure 1. As evident, the area under the curves of the peaks in the range of 1640-1820 cm^{-1} were considered to be associated with C=O stretching which increased because of the increase in carboxyl groups. Compared with the non-treated biochar (e.g., BC, C=O absorbance 47.8 a.u.), the signal increased for the samples with increased thermal treatment time (e.g., 136.4 and 152 a.u. for 3.5BC and 8BC, respectively). However, 24BC did not follow the trend showing a decreased amount of C=O groups (78.4 a.u.), but an increased amount of C–O groups. The peak around 1060 cm^{-1} in the FTIR spectrum (Figure 1) and the increase in the signal centered at 1735 cm^{-1} could be the reason for the observed increase in the hydrophilicity of the thermally treated samples compared to the non-thermally treated biochar (BC), as reported previously [10]. These results are in agreement with a study where thermal treatment was shown to have a significant effect on drop penetration time and contact angle in biochar prepared from poultry litter [28]. In their study, Yi et al. [28] suggested that the hydrophobicity of the biochar surface was associated with some semivolatile organic compounds (e.g., 1,3-bis(1,1-dimethylethyl)-benzene, 2,5-bis(1,1-dimethylethyl)-phenol, tetradecane, and octacosane) coating the surface of the material. The effect of having a close interaction between water and the surface of thermally treated biochars would be expected to produce relatively faster diffusion of water-soluble chemical species attached to the solid surface.

The increase in the bands associated with C=O and C–O has been suggested in past research as being related to oxidation of the biochar surface and subsequent generation of active adsorption sites [29]. In agreement with Fahmi et al. [29], biochar with a lower amount of oxidized sites will show relatively lower cation exchange capacity (CEC) compared to biochar with a higher oxidized surface. As described above, samples in this study were thermally treated after pyrolysis under ambient conditions, meaning that oxidation of the biochar surface is highly likely during additional

thermal treatment, as suggested by the increased C=O and C−O absorption bands. The higher oxidation surface in biochar would be able to retain contaminants because of its higher capability to interact with the functional groups remaining on the surface. A reduction in the 1430 cm^{-1} band observed in the FTIR analysis (Figure 1) also support the surface oxidation hypothesis.
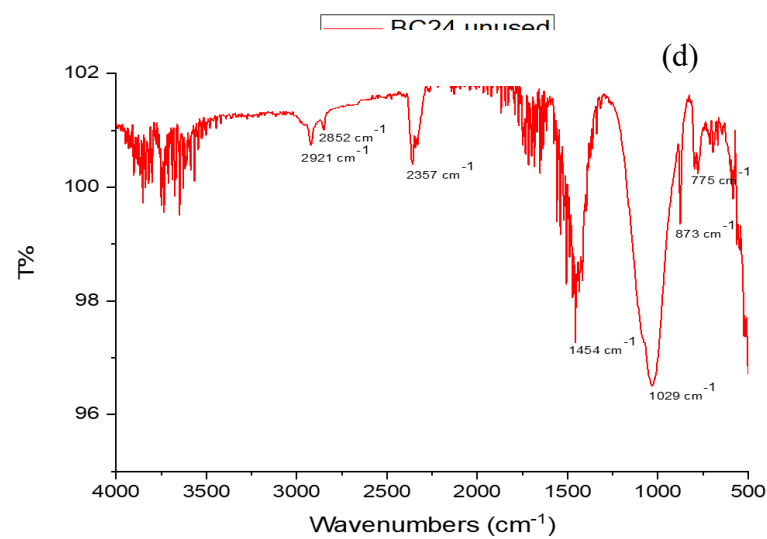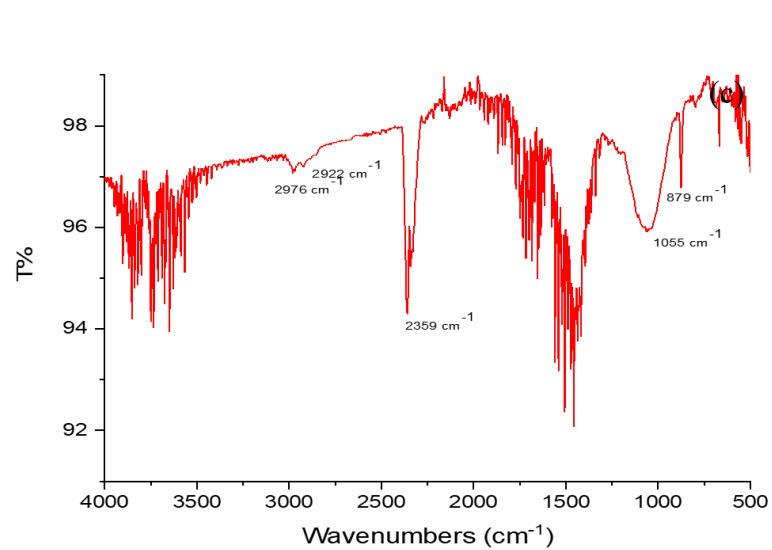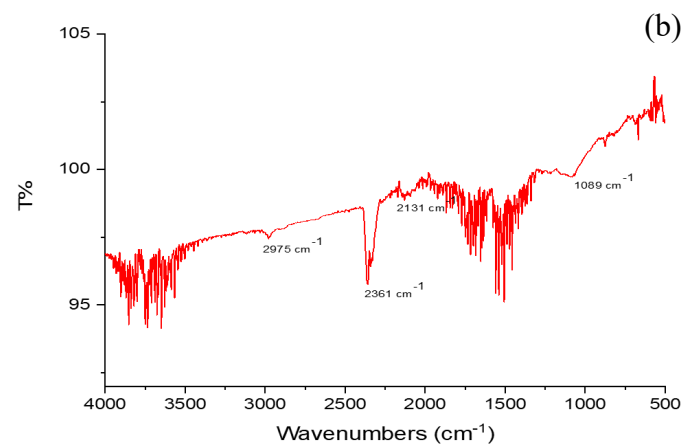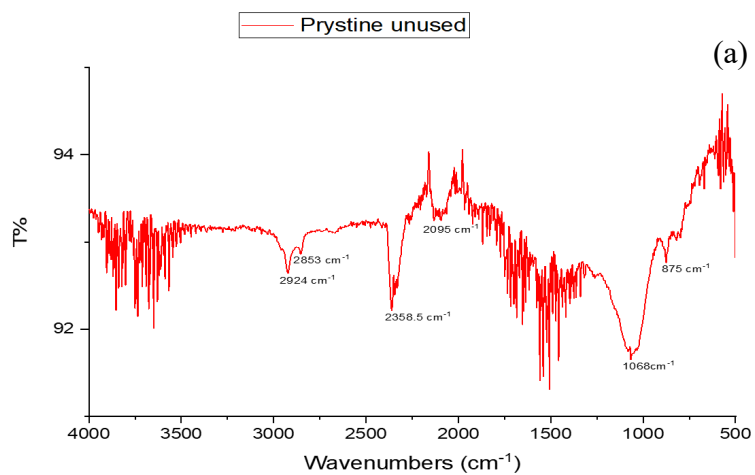
Figure 1. FTIR spectra for: (a) BC, (b) 3.5BC, (c) 8BC, and (d) 24BC.

The XRD patterns of non-thermally treated (BC) and 300°C thermally treated 3.5, 8, and 24 hours biochars (3.5BC, 8BC, and 24BC, respectively) are shown in Figure 2. The XRD pattern is dominated by the crystalline cellulose in the original biomass with a signal centered around 27° corresponding to the (002) reflection as the most predominant [30]. Higher peak density was observed in BC, compared with the 3.5 hours thermally treated biochar (3.5BC), thus indicating a higher crystalline structure being present in the untreated material. The XRD pattern for 8BC and 24BC showed higher peak density compared to 3.5BC, suggesting a recovery of the crystalline structure being higher for 8BC when compared with 24BC. The signal centered on 20° is considered to be related to the (220) reflection, which appears as very small for 3.5BC compared to the untreated, 8BC, and 24BC materials. This behavior has been explained before in terms of the disappearance of crystalline cellulose pattern and consistent with a secondary phase transition as the structure of the biochar starts moving from a transition char towards a disordered char [31]. As the thermal treatment time increases, some biomass structure degradation may be observed along with the increase in carbon content. Results shown in Figure 2 suggest that, after a transformation period occurring when the biochar is thermally treated at 300°C for 3.5 hours, the transition is completed after 8 hours of treatment and continues when the biochar treatment is prolonged until 24 hours. This transitional stage for 3.5BC is also corroborated by the decrease in the signal centered at 50° in 8BC, and 24BC, related to the (100) reflection after thermal treatment as shown for 3.5BC in Figure 2. The other signals observed in the XRD analysis could be related to the presence of SiO_2 or calcite, as previously reported for pine bark biochar prepared under similar conditions [32].

As described in Section 2.1, BC was produced at 600±50 °C and under low oxygen atmosphere suggesting a significant content of sp^2 carbon and the incipient formation of graphene layers [31]. When the post-pyrolysis thermal treatment was applied to BC to generate 3.5BC, 8BC, and 24BC, the uncontrolled presence of oxygen may lead to the generation of graphene oxide-type structures which have been reported with an increased capacity for interaction with contaminants [33] and wettability compared with BC. These results are in agreement with other studies on the generation of oxygen-containing functional groups in carbon-based materials. For example, Chen et al. [34] suggested that graphitic sp^2 carbon is likely to produce C=O groups when longer duration/lower temperature thermal treatment is used and more C-O-C groups when shorter duration/higher temperature treatment is used for annealing carbon nanotubes. The proposed mechanism for C=O groups by these researchers involved 1,2 peroxidation followed by homolytically breaking of C-C and -O-O- bonds, which is thermodynamically favored at lower temperature because of the lower activation energy for 1,2 peroxidation with planar graphitic ring. Figure S1 in the Supplementary Information shows a schematic overview of the mechanisms of C=O groups in thermally treated biochars based on the hypothesis suggested by Chen et al. [34].

The layer coherence length (t_{002}) in the different biochars was estimated using the Scherer equation and the average distance between the two adjacent planes (d_{002}), also known as interlayer spacing, was obtained from Bragg's law [31]. The average number of graphene layers was estimated by the ratio between the layer coherence length and interlayer spacing. Additionally the crystallinity index (CI) for the different materials was estimated using the methodology proposed by Chandra and Bhattacharya [35]. The estimated values are shown in Table S1 in the Supplementary Information. The loss of crystalline cellulose XRD pattern during pyrolysis of biomass has been described in past literature [31], suggesting that the changes to the material structure are associated with the decrease in the layer coherence length values of the biochar. In our work, t_{002} value of BC

was 1.42 nm, which is in the same order of magnitude as reported for biochar produced from wood feedstock under similar temperature conditions (e.g., 1.9 nm) [31]. We found a slight decrease in crystallinity as the raw biochar was thermally treated at 300°C for 3.5 h, followed by an increase in the CI values until a value higher than the initial value for the 24BC biochar. The variability in the CI values reported in Table S1 are in agreement with other studies [35], where the residence time was found to exert a significant influence on the CI for different biochars for the same temperature treatment. In general, Chandra and Bhattacharya [35] found a slight decrease in the CI value when the detention time increased. However, these researchers only reported detention times in the range of 60-120 min.
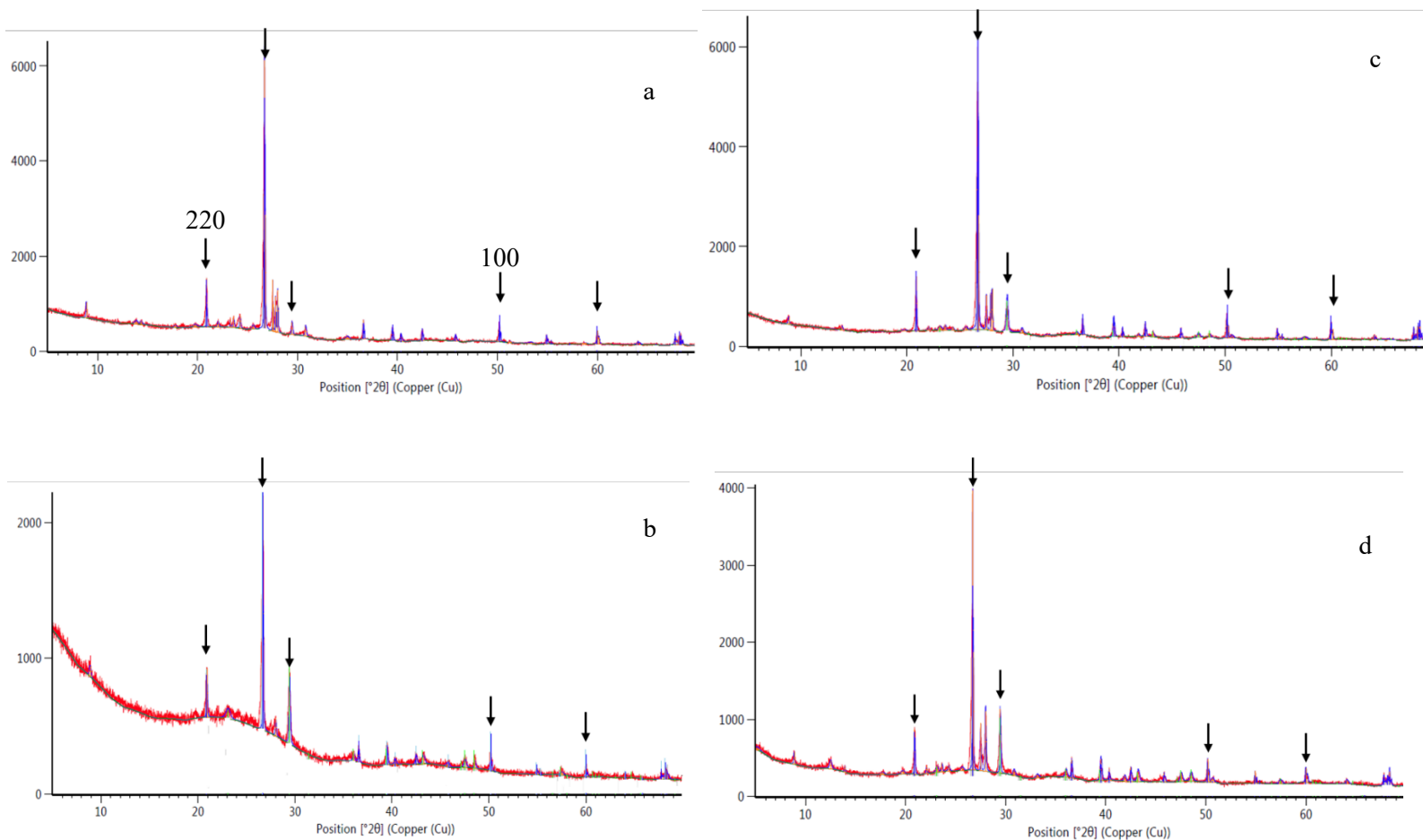
Figure 2. The X-ray diffractometer (XRD) pattern: (a) non-thermally treated biochar (BC), (b) 3.5 hours 300°C thermally treated biochar (3.5BC), (c) 8.0 hours 300°C thermally treated biochar (8BC), (d) 24 hours 300°C thermally treated biochar (24BC).

When secondary post-pyrolysis thermal treatment was applied, the t_{002} values decreased related with the transition from disordered char to composite char, and then increased again slightly, in this case not as a function of the increase in carbonization temperature, but as a function of treatment time [31]. In the same way, the decrease in the (100) layer coherence length (see Table S1), also point to more ordered carbon clusters with increased sp^2 content, but with a stable number of graphene layers.

3.2 ACT adsorption

Figure 3 shows ACT adsorption curves for the different biochar materials (e.g., BC, 3.5BC, 8BC, and 24BC) tested at the highest load (2 g L^{-1}). The lowest ACT adsorption was observed when BC was tested, when the overall ACT adsorption was found to be 11% after 60 minutes, suggesting that hydrophobic surface of BC did not efficiently attract ACT molecules.

It is important to note that ACT adsorption increased significantly with the post-pyrolysis thermal treatment applied. When 3.5BC was used, the overall ACT adsorption was found to be as high as 39%, which is over three folds higher than the value achieved with BC. Further increase in the thermal treatment time produced an additional increase in ACT removal. The highest removal was achieved using the 24BC (50%), closely followed by 8BC (47%).

After initial exploration of the capability of the different biochar materials, a decision was made to select 8BC to further continue with the assessment of biochar capability for adsorption. This is because, as shown in Figure 3, the material thermally treated at 300°C for 8 hours showed almost the same removal efficiency as the material generated after 24 hours of thermal treatment, but using one third of the amount of energy required. Figure 4 shows the results obtained when 8BC was tested for the adsorption of ACT using different adsorbent loads (0 to 6 g L^{-1}).
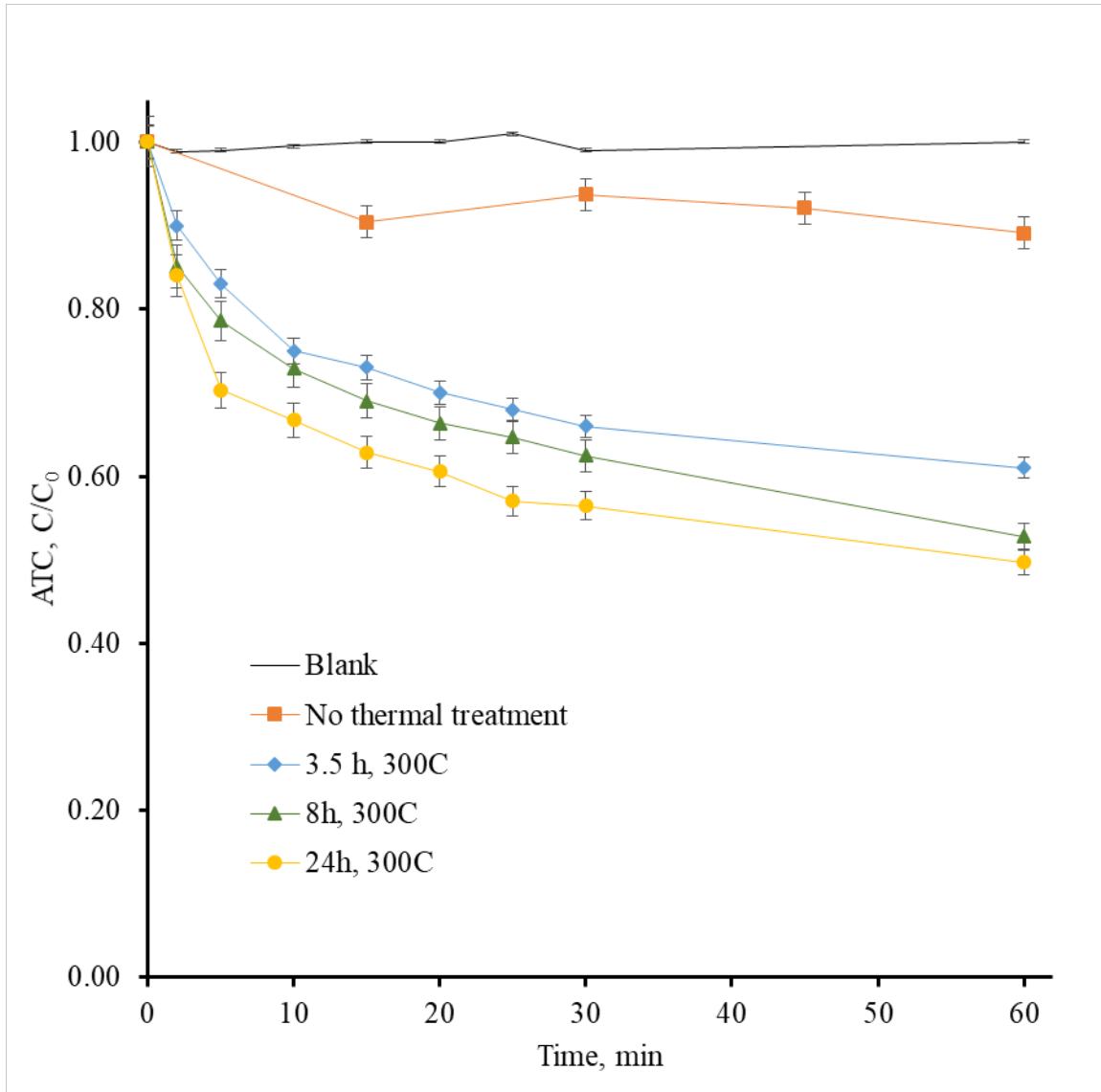
Figure 3. Adsorption of ACT for the different biochar materials with no treatment and after 3.5, 8, and 24 h thermal treatment at 300°C using biochar load of 2 g L^{-1} and ACT initial concentration of 0.66 mM (100 mg L^{-1})

As shown in Figure 4, the adsorbent load has a significant effect on ACT adsorption with the best performance achieving up to 91% ACT removal within 90 minutes of contact time when 6 g L^{-1} of 8BC were used, followed closely by the removal achieved using 4 g L^{-1} (74%), and eventually removals achieved using 2, 1 and 0.5 g L^{-1} (e.g., 55, 49, and 20%, respectively after 90 minutes). In order to perform a fair comparison of the performance of the different materials tested, the Langmuir and Freundlich isotherm models were tested to fit the experimental results obtained.
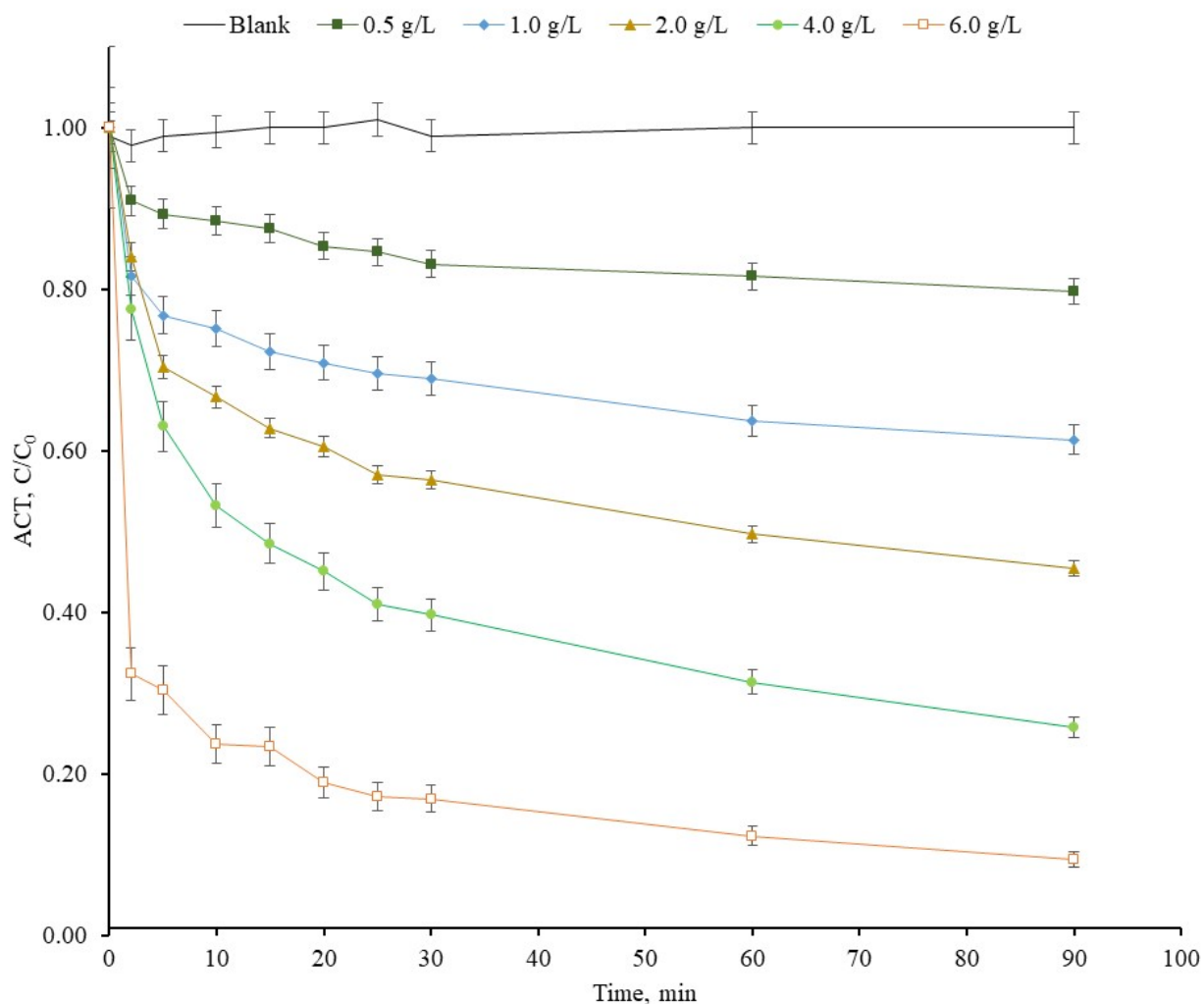
Figure 4. Effect of biochar load (8BC, 0.5-6.0 g L^{-1}) on ACT removal (initial concentration 0.66 mM) adsorption at 20°C.

Table 1 includes the parameters of the two adsorption isotherm models tested. As shown, the Langmuir isotherm model was the best fit for the experimental data set in all the cases showing the highest correlation coefficient values, suggesting that the surface contains adsorbing sites, energetically equivalent and with the same energy of adsorption, and the generation of a monolayer coverage [36]. The best fit of the Langmuir isotherm model agrees with the characterization of the surface functional groups described above for the different materials tested, as the increase in oxygen-containing functional groups appear to be not only responsible for the changes in the hydrophobicity/hydrophilicity balance on the biochar surface, but also for the interaction with ACT molecules to generate the monolayer indicated by the Langmuir model. Using the Langmuir isotherm parameters in Table 1, the reparation factor (R$_L$) was calculated as the way to compare the capability of the different materials for ACT adsorption, as reported previously [37]. In agreement with Ayawei et al. [37], R$_L$ values indicate the adsorption to be unfavorable when R$_L$ > 1, linear when R = 1, favorable when 0 < R$_L$< 1, and irreversible when R$_L$ = 0. From the results given in Table 1, adsorption was

favorable for all the cases, with the most linear value assigned to the adsorption process using 8BC ($R_L = 1.2 \times 10^{-4}$) being twice as much as the other R_L values estimated for the other materials, suggesting it performs best for ACT adsorption.

Table 1. Adsorption isotherm results for ACT removal using 8BC.

Biochar type	Langmuir				Freundlich		
	Q_m, mgg^{-1}	k_L, mgL^{-1}	$R_L/10^5$	R^2	n	K_e	R^2
BC	24.63	135.58	6.2	**0.96**	0.22	1.03×10^{-7}	0.85
3.5BC	3.83	127.76	5.6	**0.999**	0.37	5.34×10^{-5}	0.97
8BC	1.02	62.48	12.0	**0.9995**	0.65	9.74×10^{-5}	0.97
24BC	3.16	108.35	6.7	**0.9995**	0.36	2.61×10^{-5}	0.97

The results from the adsorption isotherm model are also supported by the characterization of the different materials. For example, from Figure 1, 8BC was found to be the biochar with the highest amount of oxygen-containing functional groups for both C=O and C-O bonds. It would be expected that the oxygen-containing functional groups would be able to interact forming hydrogen bonds with the amide and hydroxyl groups in ACT generating weak interaction, but strong enough to enhance ACT adsorption [38]. The type of interactions between the functional groups on the surface of biochar and ACT is shown in Figure 5a, where chemisorption through hydrogen bonding-type interaction between the chemical species is schematically displayed. Also, the interlayer spacing for the thermally treated biochars was large enough to allow interaction of the chemical species between the graphene layers produced (see also Figure 5), considering ACT as a fairly plane, small molecule (8.5×5.7 Å^2) [39].

The characterization of the materials using XPS and other conventional characterization technologies (e.g., SEM, TEM/EDS, ICP-OES) is reported elsewhere [10]. The results strongly support the findings on ACT adsorption by showing how texture in the heat treated biochars has changed by changing the heating time using TEM analysis, and the increased presence of oxygen-containing groups as the thermal treatment time increases. The increased amount of carbonyl groups on the surface of the thermally treated biochars was also suggested by XPS analysis to enhance the stabilization of zero-valent iron nanoparticles by fast formation of a stable Fe^{3+} layer coating through fast oxidation induced by the carbonyl groups. In their work, Mortazavian et al. [10] concluded that alterations to the surface functional groups, and surface charges in thermally treated biochars enhance their interaction with aqueous contaminants and increase the number of adsorption sites suitable for ACT adsorption, such as in the case of this research study.

Additional to the adsorption isotherm models, the Lagergren models for pseudo-first, and pseudo-second order kinetics were also used to describe the adsorption process of ACT by the different biochars. The best fit was achieved using the pseudo-second order kinetics, compared with the pseudo-first order kinetics, suggesting that chemisorption is the rate-limiting step in the adsorption process and that the adsorption rate will mostly depend on the sorption capacity of the biochar, but not on the concentration of the sorbate [40]. Table 2 shows the results of applying the model to the experimental data set. As shown, the highest rate constant value was observed when using 8BC with the highest load (6 g L^{-1}) for which a value as high as 0.021 g mg^{-1}min^{-1} was obtained.

Further decrease in the 8BC load showed the trend to significantly decrease the rate constant value until reaching its lowest value for the lowest 8BC load (0.5 g L^{-1}) tested as 0.002 g mg^{-1}min^{-1}, one order of magnitude smaller. The variation in sorption capacity and ACT removal as a function of the 8BC load is shown in Figure 6 where the effect of ionic strength on these parameters is also displayed. As evident, by increasing the 8BC dose from 0.5 to 6 g L^{-1}, the equilibrium sorption capacity, q_e, decreased from 56.5 to 22.0 mg g^{-1}. However, the removal of ACT increased from 20 to 91% with the same increase. The relationship between the equilibrium sorption capacity, q_e, and the 8BC dose was found to fit a linear regression with a fair coefficient of determination value (R^2=0.91), which can be expressed as q_e = S8BC + Y where the constant, Y, 56.8 mg g^{-1} is the maximum sorption capacity, when the biochar load approaches zero, and S at -6.5 L mg g^{-1} is related to the sorption potential of the material.

(a)
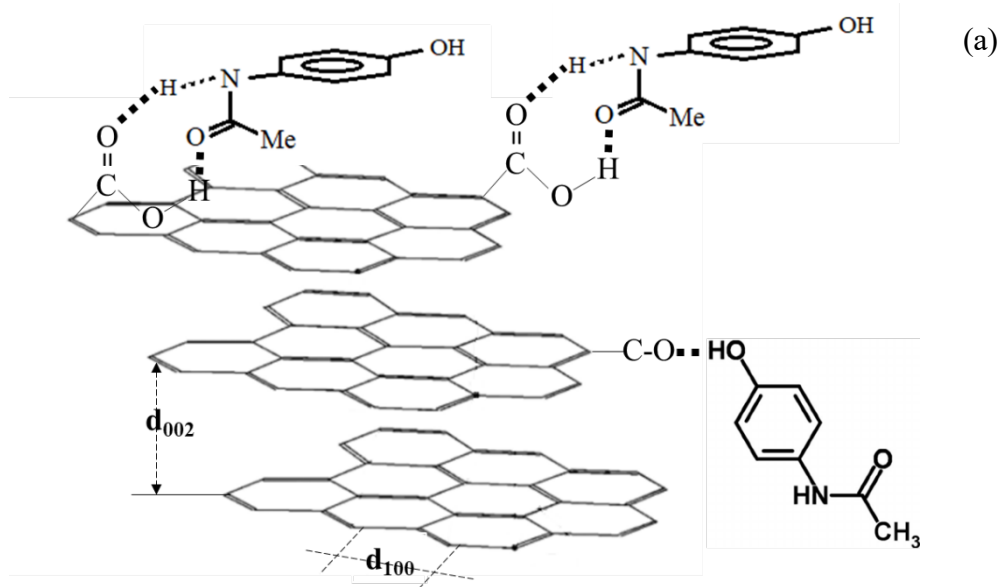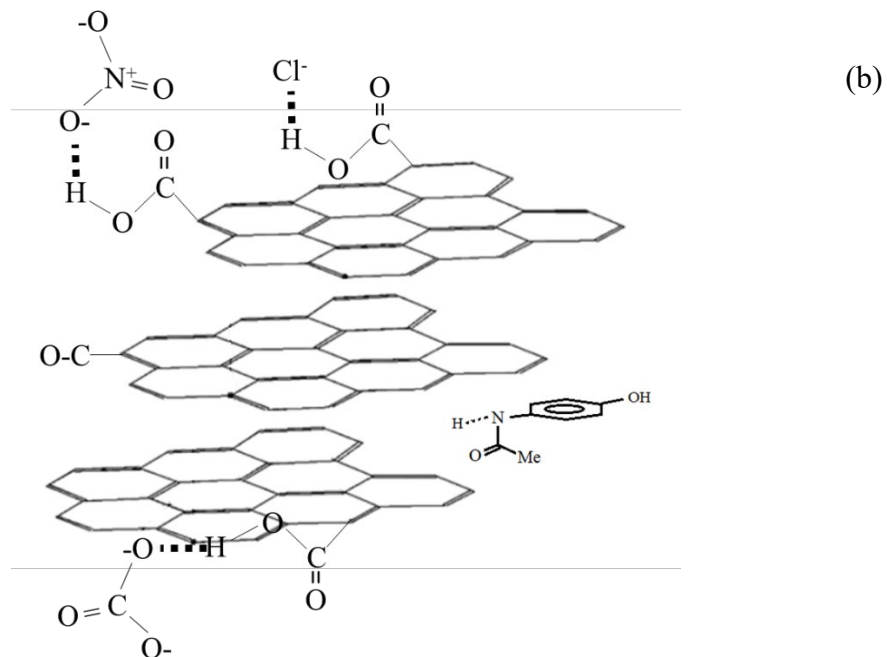
Figure 5. Schematic representation of the interaction between oxygen-containing functional groups on the surface of biochar and ACT molecules: (a) absence, and (b) presence of chloride, carbonate, and nitrate ion.

The negative value shows that the equilibrium sorption capacity decreases with the increase in the dose of the biosorbent [40]. Finally, only a slight variation in the initial sorption rate, h, was observed for the different biochar doses, averaging 6.8 mg g^{-1}min^{-1}(see Table 2).

Table 2. Kinetics results for the adsorption of ACT in different thermally-treated biochars.

| Biochar type	BC load, gL^{-1}	Ion/concentration, mM	Lagergren equation	q_e, mgg^{-1}	k_2, gmg^{-1}min^{-1}	h, mg g^{-1}min^{-1}	R^2
3.5BC	0.5	Null	$1/qe = 0.017t + 0.03$	56.5	0.0098	31.3	0.998
	1.0	Null	$1/qe = 0.024t + 0.09$	40.2	0.0063	10.2	0.997
	2.0	Null	$1/qe = 0.031t + 0.19$	32.2	0.0051	5.3	0.999
8BC	0.5	Null	$1/qe = 0.017t + 0.13$	56.5	0.0020	6.5	0.991
	1.0	Null	$1/qe = 0.019t + 0.11$	53.5	0.0031	8.9	0.95
	2.0	Null	$1/qe = 0.026t + 0.19$	38.2	0.0035	5.1	0.994
	4.0	Null	$1/qe = 0.038t + 0.28$	25.9	0.0053	3.6	0.996
	6.0	Null	$1/qe = 0.045t + 0.01$	21.9	**0.021**	10.0	0.999
24BC	0.5	Null	$1/qe = 0.013t + 0.07$	78.7	0.0021	13.4	0.987
	1.0	Null	$1/qe = 0.020t + 0.20$	50.2	0.0019	4.9	0.994
	2.0	Null	$1/qe = 0.025t + 0.24$	39.2	0.0033	5.1	0.97
8BC	6.0	[Cl$^-$], 1mM	$1/qe = 0.053t + 0.39$	18.7	0.0072	2.5	0.999
8BC	6.0	[Cl$^-$], 5mM	$1/qe = 0.071t + 1.10$	13.9	0.0026	0.5	0.996
8BC	6.0	[CO$_3$], 1mM	$1/qe = 0.052t + 0.53$	18.9	0.0052	1.9	0.991
8BC	6.0	[CO$_3$], 5mM	$1/qe = 0.101t + 0.54$	9.84	0.019	1.9	0.997
8BC	6.0	[NO$_3$], 1mM	$1/qe = 0.038t + 0.99$	26.3	0.0014	1.0	0.995
8BC	6.0	[NO$_3$], 5mM	$1/qe = 0.081t + 0.40$	12.2	0.016	2.5	0.994
8BC	6.0	[Cl$^-$]+[CO$_3$], 1 mM	$1/qe = 0.056t + 0.53$	17.8	0.0058	1.9	0.996
8BC	6.0	[Cl$^-$]+[NO$_3$], 1mM	$1/qe = 0.057t + 0.48$	17.4	0.007	2.1	0.999
8BC	6.0	[CO$_3$]+[NO$_3$], 1mM	$1/qe = 0.061t + 0.37$	16.3	0.010	2.7	0.995
8BC	6.0	[Cl$^-$]+[CO$_3$]+[NO$_3$], 1mM	$1/qe = 0.064t + 0.41$	15.6	0.009	2.4	0.999
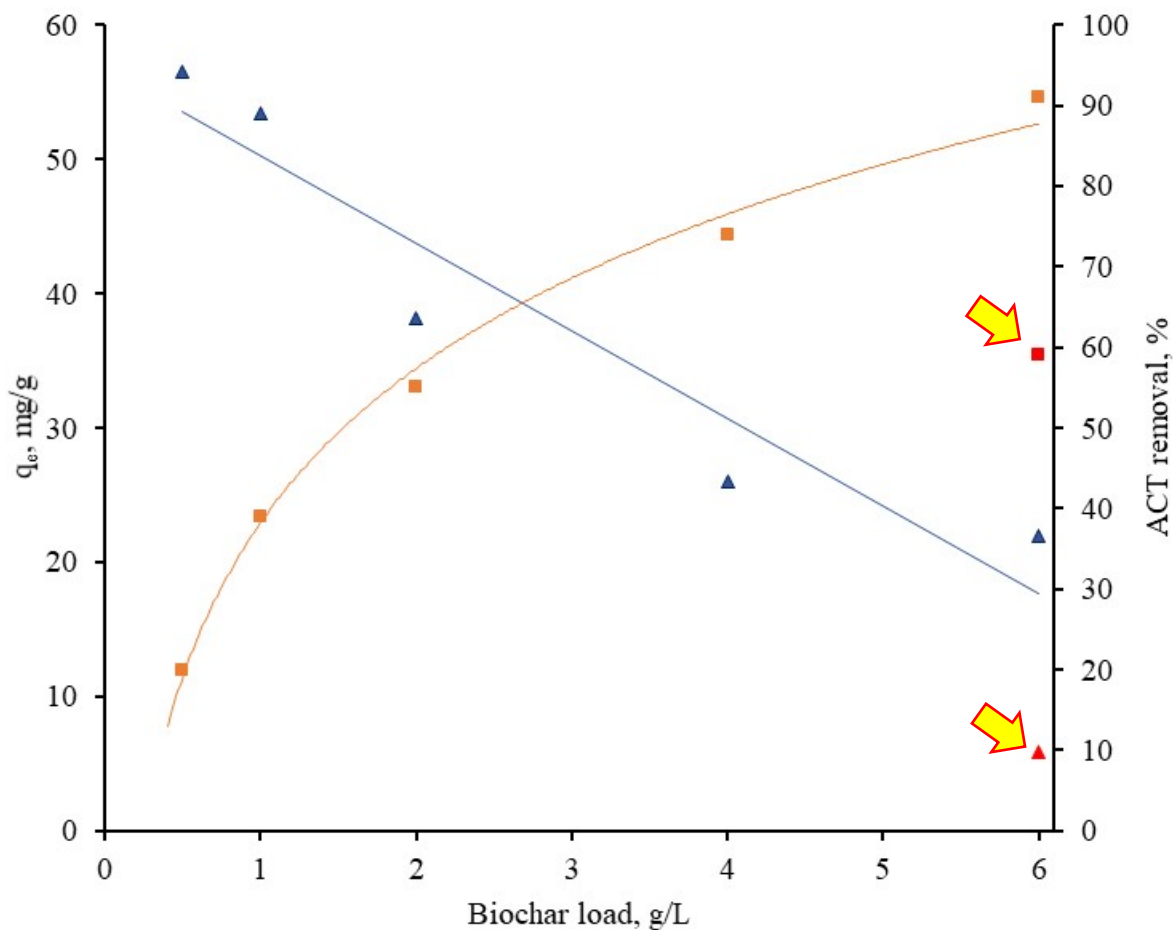
Figure 6. Variation in sorption capacity and ACT removal as a function of the 8BC load and the effect of ionic strength (The red square and triangle pointed by the yellow arrows are the results obtained when ions were present in solution).

3.3 Effect of the presence of anions in the solution

The effect of addition of different ions to the tested concentrations is illustrated in Figure 7. Figure 7a shows the effect of the individual ions (i.e., chloride, carbonate, and nitrate) for the two concentrations tested (1.0 and 5.0 mmol L^{-1}), while Figure 7b shows the effect of combination of two or three ions using 1 mmol L^{-1} of each and 6 g L^{-1} of 8BC. The ACT adsorption curve using deionized water (no ions added) for the same test conditions is also shown for comparison purposes.
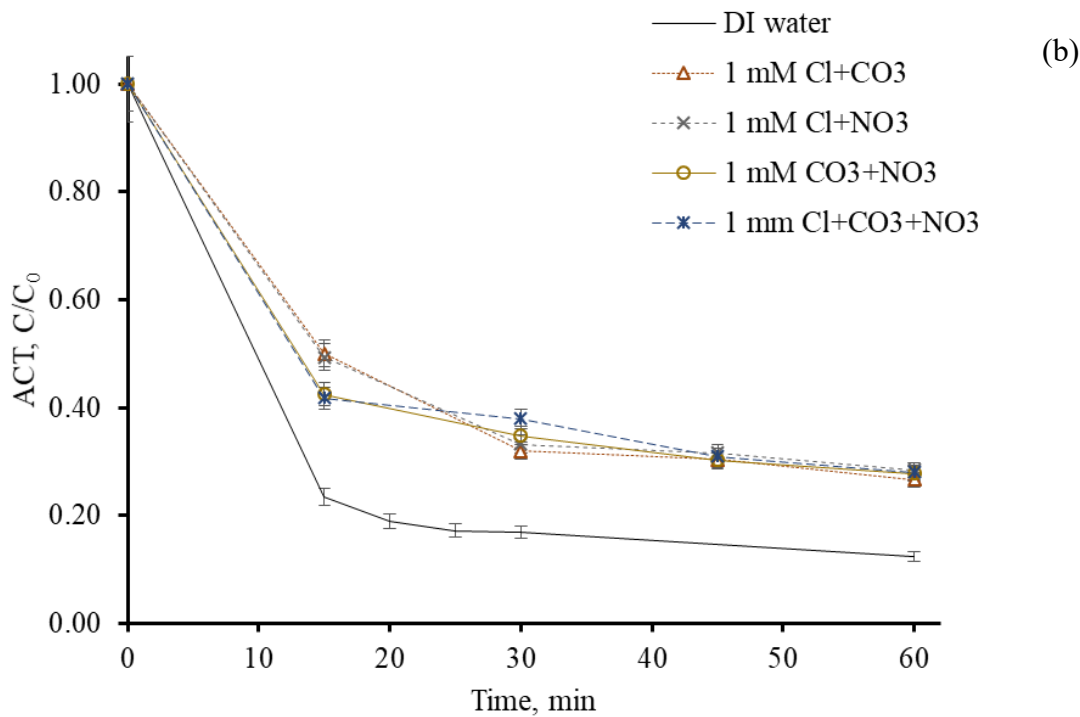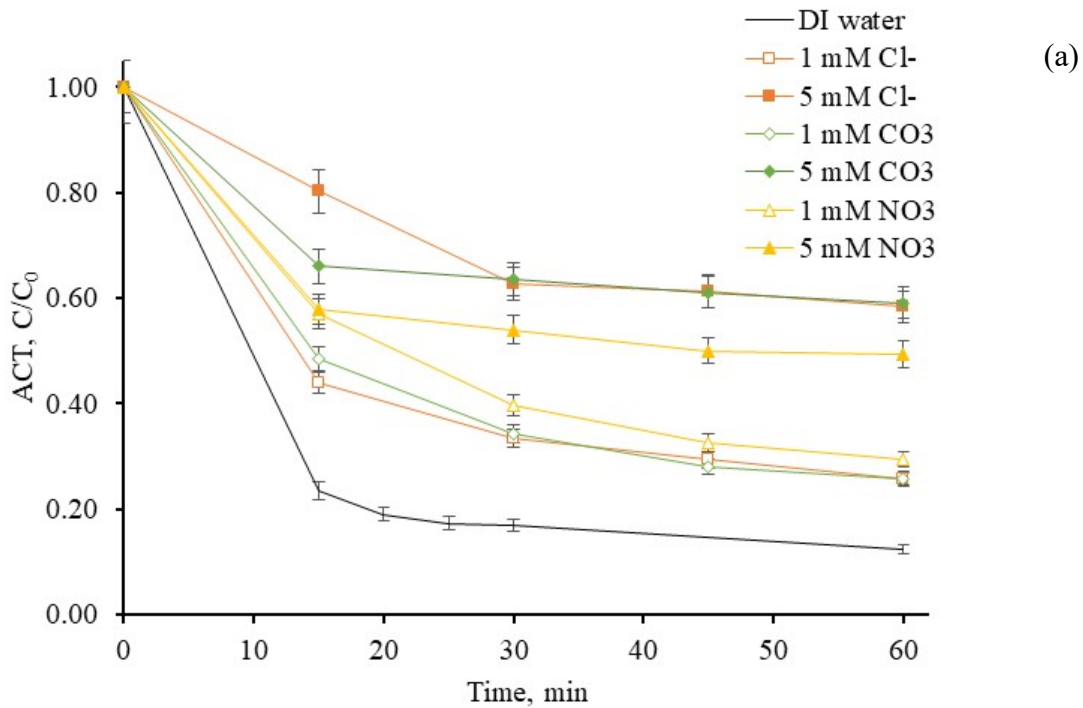
Figure 7. Effect of ionic strength: (a) individual ions, (b) combined ions on ACT adsorption in 8BC.

As shown in Figure 7a, addition of any of the tested ions to any of the tested concentrations exerted a significant influence on the ACT adsorption process when compared with DI water. The effect of the ions can be explained as the interaction of these chemical structures with the functional groups on the surface of the biochar which impeded the interaction with ACT molecules, as

suggested in Figure 5b. The effect of the individual ions was also observed when the Lagergren kinetic values were estimated for the ACT adsorption curves. For example, the adsorption rate decreased from 0.021 g mg^{-1}min^{-1} for the 8BC in deionized water to 0.0072 and 0.0026 when 1 and 5 mM of chloride were added. In the case of carbonate and nitrate, the effect of adding 1 mM showed the highest impact in both cases, and further increase in the concentration to 5 mM did not show the same decrease in the adsorption rate as observed for chloride, but a slight increase, which is attributed to the steric effect as carbonate and nitrate ions are significantly bigger than chloride. The same trend was found for other kinetic parameters such as h, where the values significantly decreased to as low as one order of magnitude in the case of nitrate 1 mM with the addition of the different ions at the different concentrations tested. The remaining ACT adsorption observed could be related to specific active sites that were not occupied by the ions in solution or within the interlayer space estimated as shown in Table S1.

The effect of the addition of a single ion is illustrated in Figure 6 where the assessed values of q_e and ACT removal are displayed in red and highlighted with the yellow arrow for the addition of chloride 5 mM and 8BC dose of 6 g L^{-1} as the worst case scenario. As shown, q_e decreased from 21.9 mg g^{-1} for deionized water to 9.8 mg g^{-1} when 5 mM of chloride was added, while ACT removal decreased from 91 to 59%. These results are in agreement with the proposed monolayer model for the adsorption process, because once the number of active sites are occupied by either ACT or ions, the adsorption process will stabilize reaching equilibrium and the adsorption rate will drop significantly. Additionally, as chemisorption has been suggested as the rate-limiting step in the adsorption process, the effect of ions interrupting the chemisorption of ACT molecules would be expected in generating the observed results.

The ACT adsorption curves for the experimental trials using two or more ions combined using 1 mM and 6 g L^{-1} of 8BC are shown in Figure 7b. It is important to note that the effect observed for more than one ion seems to be less than the effect of single ions as shown in Figure 7a. Most of the ACT adsorption curves shown in Figure 7b overlap and reach almost the same final removal value (c.a., 72% ACT adsorption), suggesting that the ions in the system will also compete with each other and against ACT to occupy the active sites on the surface of the biochar. The adsorption rate value, for example, decreased from 0.021 g mg^{-1}min^{-1} for DI water to 0.009 g mg^{-1}min^{-1}, which is over one order of magnitude, when the three ions (chloride, carbonate and nitrate) were added at the same time at a concentration of 1 mM.

3.4 Multivariate analysis

3.4.1 Adsorption performance of ACT for different biochar materials

Figure 8 shows the hierarchical clustering of ACT adsorption for different biochar materials, including the biochars subject to different thermal treatments (Figure 8a) and adsorbent loads (Figure 8b). In Figure 8, two primary clusters can be identified; treated and non-treated biochar, suggesting that the variability in thermally enhanced biochar can significantly influence the adsorption of ACT. These results confirm our experimental findings and its relationship with the changes observed in the frequency of oxygen-containing functional groups on the surface and the consequent change in hydrophobicity/hydrophilicity of the biochar materials generated. As evident from Figure 8a, biochar treated for 8 h and 24 h (e.g., 8BC and 24BC) are grouped together, showing a similar correlation coefficient distance, followed by biochar treated for 3.5 h. This implies that ACT adsorption in 8BC and 24 BC would be similar, as shown in Figure 3 where only

a slight difference in ACT adsorption was found between the two materials. Furthermore, the dendrogram representing different doses of 8BC shows that biochar loads of 2 g L⁻¹ and 4 g L⁻¹, and 0.5 g L⁻¹ and 1 g L⁻¹ have a close resemblance, clustering at the same correlation distance (Figure 8b). This suggests that the adsorption performance of these biochar doses would be similar. To confirm the observations derived from HCA and in order to understand the relative adsorption performance of biochar having different adsorbent characteristics, the data set was classified using PROMETHEE net ranking.
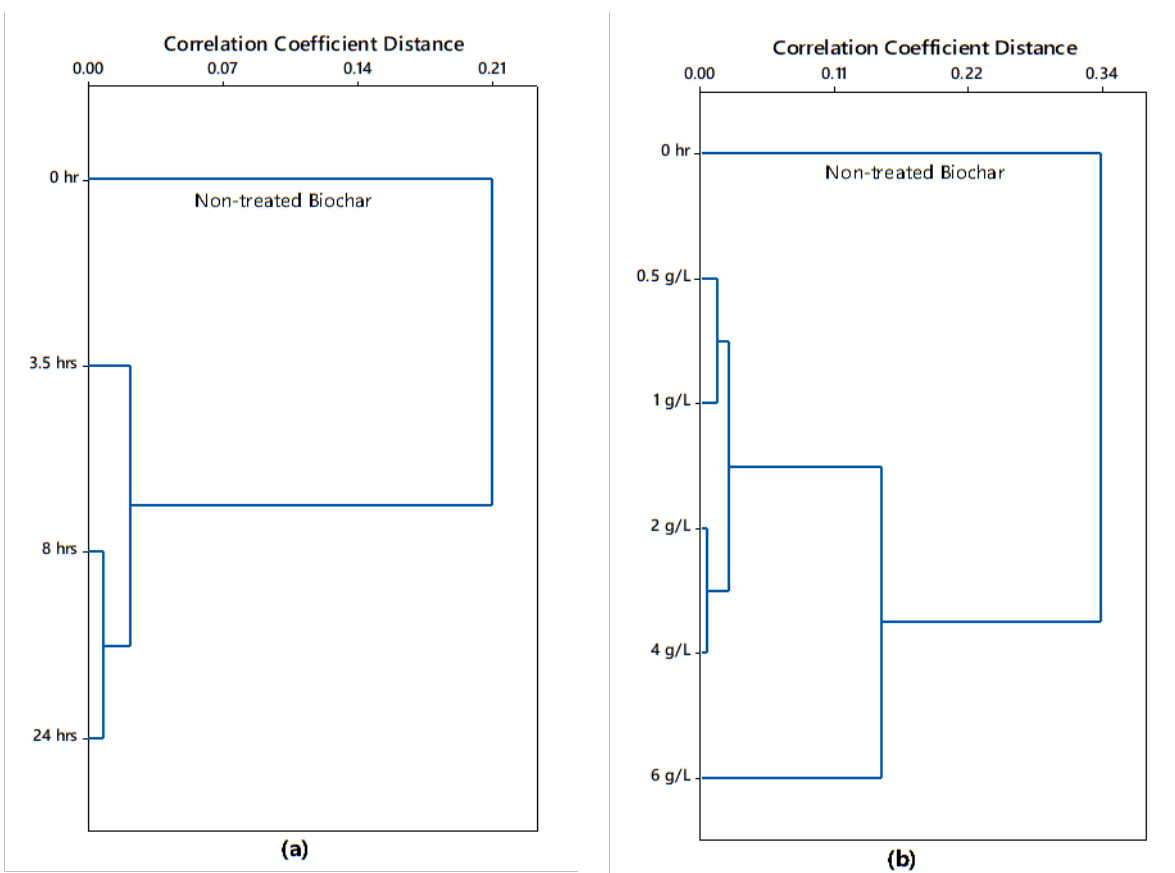

Figure 8. Dendrogram showing the clustering of treated and non-treated biochar materials based on ACT adsorption capacity: (a) biochar treated for different times, (b) different adsorbent dosage.

Equal weight was given for all variables (i.e. concentration of ACT at a given time), assuming that each time step is equally important for the adsorption process, and the linear preference function was used. As evident from PROMETHEE net ranking outcomes given in Table 3, biochar of 6 g L⁻¹ and 4 g L⁻¹ treated for 8 h ranked at the top with higher positive outranking flows (net Phi), followed by 24BC at 2 g L⁻¹. These results indicate that the adsorption capacity of 6 g L⁻¹ and 4 g L⁻¹ of 8BC is high compared to 24BC when a dose of 2 g L⁻¹ is used. Nevertheless, when the same dose of biochar was used (e.g., 2 g L⁻¹), 24BC out-performed 8BC suggesting that longer the thermal treatment time, will produce higher hydrophilic surfaces suitable for enhanced pollutant adsorption, and that increased loads of the sorbent will enhance the overall amount of ACT

21

adsorbed, as evident from the adsorption isotherm and kinetic models proposed. This is also evident from the GAIA biplot given in the Supplementary Information (Figure S2), where the decision axis is directed towards the objects related to 6 g L^{-1} and 4 g L^{-1}, indicating that the biochar as treated are the most favorable for the adsorption of ACT. Table 4 also shows that the adsorption of ACT by 8BC at 0.5 g L^{-1} is the lowest among the samples (i.e. high negative Phi values) and it also shows a lower performance compared to non-treated biochar. This is attributed to the lower dosage of biochar for ACT adsorption compared to the non-treated biochar (2 g L^{-1}). These results further confirm our finding that even though thermally treated biochar can increase the adsorption of ACT, the adsorbent dosage is an essential parameter when determining the adsorption performance.

Table 3. PROMETHEE net ranking outcomes for different biochar (BC) materials.

Objects	Rank	Net Phi
6 g L^{-1}_8 h	1	0.7480
4 g L^{-1}_8 h	2	0.2632
24BC_2 g L^{-1}	3	-0.0173
2 g L^{-1}_ 8 h	3	-0.0173
8BC_2 g L^{-1}	5	-0.1163
1 g L^{-1}_8 h	6	-0.1582
3.5BC_8 h	7	-0.1602
Untreated BC	8	-0.1974
0.5 g L^{-1}_8 h	9	-0.3444

3.4.2 Effect of ionic strength

The effect of the addition of ions at different concentrations on the adsorption performance of ACT was investigated using PROMETHEE ranking (Table 4) together with GAIA analysis (Figures S3-S4). In this analysis, the effect of ions was ranked considering two different systems; single ions and multiple ions, along with the solution having no influential ions (DI water). As evident from the ranking outcomes for single and multiple ion systems, the solution with no influential ions is top ranked with higher positive net Phi values, followed by different ionic strengths, suggesting that the adsorption capacity of ACT decreases with the influence of different ions. GAIA biplots also show the decision power of objects related to 'no ions' compared to the other objects (Figures S3-S4).

In the single ion system, the adsorption capacity of ACT decreases in the order of Cl > CO$_3$ > NO$_3$ in 1 mM concentration, whilst it follows the order: NO$_3$ > CO$_3$ > Cl when the ionic concentration becomes 5 mM (Table 4). This trend could be explained considering firstly, the electronegativity of the ionic species involved and secondly, their actual ionic radii. When the ions are used at low concentration, chloride was found to have the highest influence because it is more electronegative than nitrate and carbonate ions, able to attach to the oxygen-containing functional groups on the surface of the biochar and decreasing their capability to interact with ACT molecules. As the added concentration of the ions increased to 5 mM, the effect of electronegativity decreases and the steric

effect becomes predominant with nitrate and carbonate becoming more influential, as the ions with the bigger topological polar surface area interfere more significantly compared to the chloride ion, which is considered to have zero topological polar surface area.

Table 4. PROMETHEE net ranking outcomes for ACT adsorption in biochar in the presence of ions.

Single ion system			Multi ion systems		
Objects	Rank	Net Phi	Objects	Rank	Net Phi
No ions	1	0.4954	No ions	1	0.1941
Cl_1mM	2	0.3345	CO_3+NO_3_1mM	2	-0.042
CO_3_1mM	3	0.319	CO_3+NO_3+Cl_1mM	3	-0.0476
NO_3_1mM	4	0.1544	NO_3+Cl_1mM	4	-0.051
NO_3_5mM	5	-0.2773	CO_3+Cl_1mM	5	-0.0535
CO_3_5mM	6	-0.4778			
Cl_5mM	7	-0.5481			

PROMETHEE ranking for multiple ion systems given in Table 4 indicates that the adsorption capacity of ACT follows the order: no ions > [CO_3 and NO_3] > [Cl and NO_3 and CO_3] > [NO_3 and Cl] > [CO_3 and Cl]. These results suggest that the effect of increased interaction related with a higher electronegativity possess greater significance than the steric effect discussed above. The best ACT adsorption conditions were the absence of ions when deionized water was used, followed by the combination of carbonate and nitrate ions, with a significant value of topological polar surface area, but the greatest effect was noted for the mix of anions where chloride was included, enhancing the chemisorption of highly electronegative chloride ions against the interaction with ACT molecules.

4. Conclusions

The application of post-pyrolysis thermal treatment to biochar produced from pine timber was carried out to generate materials with different hydrophilic/hydrophobic properties, crystalline structures, and functional groups on the surface. The following are the main findings after testing the materials obtained for the adsorption of acetaminophen (ACT) in aqueous phase:

- The observed changes to hydrophobicity/hydrophilicity in the materials after different thermal treatment times correlated with changes in absorbance bands corresponding to oxygen-containing functional groups (e.g., C=O, C-O) on the surface of the different biochars and transformations of their crystalline pattern, including the content of sp^2 carbon and formation of graphene layers.
- The increase in post-pyrolysis thermal treatment time increased the ability of biochar to adsorb ACT. This is attributed to the increase in hydrophilicity of the surface, layer coherence length and distance between adjacent planes of the different biochars. Biochar treated for 8 h and 24h were found without significant difference in their performance for ACT adsorption. These findings suggest that energy savings can be achieved by using the 8 h thermally treated biochar (8BC) without sacrificing the treatment performance.

- The use of adsorption isotherm and kinetic models found that the adsorption process involves the generation of an adsorbate monolayer and follows pseudo-second order kinetics, suggesting chemisorption is the rate-limiting step in the process.
- The addition of different ions, separated or combined, generated a significant decrease in the adsorption capability of 8BC. For the single ion system, the adsorption capacity of ACT decreased in the order of $Cl > CO_3 > NO_3$ when 1 mM concentration was tested, while the opposite was found true when 5 mM of the different ions were tested. This trend is related to the electronegativity of the ionic species and ionic radii.
- The adsorption capacity of ACT follows the order: no ions > $[CO_3$ and $NO_3] > [Cl$ and NO_3 and $CO_3] > [NO_3$ and $Cl] > [CO_3$ and $Cl]$ suggesting that the effect of increased interaction related to higher electronegativity has greater significance than the steric effect.

Acknowledgments

References

[1]   I. Ramírez-Sánchez, E. Bandala, Photocatalytic Degradation of Estriol Using Iron-Doped TiO2 under High and Low UV Irradiation, Catalysts. 8 (2018) 625. doi:10.3390/catal8120625.

[2]   H.N. Tran, F. Tomul, N. Ha, D.. Nguyen, E.C. Lima, G.T. Le, C. Chang, V. Masindi, S.H. Woo, Innovative spherical biochar for pharmaceutical removal from water : Insight into adsorption mechanism, J. Hazard. Mater. 394 (2020) 122255. doi:10.1016/j.jhazmat.2020.122255.

[3]   O.M. Rodríguez-Narvaez, R.D. Rajapaksha, M.I. Ranasinghe, X. Bai, J.M. Peralta-hernández, E.R. Bandala, Peroxymonosulfate decomposition by homogeneous and heterogeneous Co : Kinetics and application for the degradation of acetaminophen, J. Environ. Sci. 93 (2020) 30–40. doi:10.1016/j.jes.2020.03.002.

[4]   M.E. Letelier, M. Lopez-Valladares, L. Peredo-Silva, D. Rojas-Sepulveda, P. Aracena, Microsomal oxidative damage promoted by acetaminophen metabolism, Toxicol. Vitr. 25 (2011) 1310–1313. doi:10.1016/j.tiv.2011.04.022.

[5]   B. Nunes, J. Nunes, A.M.V.M. Soares, E. Figueira, R. Freitas, Toxicological effects of paracetamol on the clam Ruditapes phillippinarum: exposure vs recovery, Aquat. Toxicol. 192 (2017) 198–206.

[6]   S.C. Antunes, R. Freitas, E. Figueira, F. Goncalves, B. Nunes, Biochemical effects of acetaminophen in aquatic species: edible clams Venerupis decussata and Venerupis philippinarum, Environ. Sci. Pollut. Res. 20 (2013) 6658–6666. doi:10.10007/s11356-013-1784-9.

[7]   X. Duan, K. O'Donnell, H. Sun, Y. Wang, S. Wang, Sulfur and Nitrogen Co-Doped Graphene for Metal-Free Catalytic Oxidation Reactions, Small. 11 (2015) 3036–3044. doi:10.1002/smll.201403715.

[8]   X. Duan, H. Sun, Y. Wang, J. Kang, S. Wang, N-doping-induced nonradical reaction on single-walled carbon nanotubes for catalytic phenol oxidation, ACS Catal. 5 (2015) 553–559. doi:10.1021/cs5017613.

[9]   X.J. Zhou, P.H. Shi, Y.F. Qin, J.C. Fan, Y.L. Min, W.F. Yao, Synthesis of Co3O4/graphene composite catalysts through CTAB-assisted method for Orange II

degradation by activation of peroxymonosulfate, J. Mater. Sci. Mater. Electron. 27 (2016) 1020–1030. doi:10.1007/s10854-015-3847-9.

[10]   S. Mortazavian, T. Jones-Lepp, J.H. Bae, D. Chun, E.R. Bandala, J. Moon, Heat-treated biochar impregnated with zero-valent iron nanoparticles for organic contaminants removal from aqueous phase: Material characterizations and kinetic studies, J. Ind. Eng. Chem. 76 (2019) 197–214. doi:10.1016/j.jiec.2019.03.041.

[11]   X. Wang, R. Yin, L. Zeng, M. Zhu, A review of graphene-based nanomaterials for removal of antibiotics from aqueous environments, Environ. Pollut. 253 (2019) 100–110. doi:10.1016/j.envpol.2019.06.067.

[12]   X. Chen, W. Da Oh, T.T. Lim, Graphene- and CNTs-based carbocatalysts in persulfates activation: Material design and catalytic mechanisms, Chem. Eng. J. 354 (2018) 941–976. doi:10.1016/j.cej.2018.08.049.

[13]   S. Gurunathan, M.A. Iqbal, M. Qasim, C.H. Park, Evaluation of Graphene Oxide Induced Cellular Toxicity and Transcriptome Analysis in Human Embryonic Kidney Cells, Nanomaterials. 9 (2019) 969. doi:10.3390/nano9070969.

[14]   K. Pikula, V. Chaika, A. Zakharenko, Z. Markina, A. Vedyagin, V. Kuznetsov, A. Gusev, S. Park, K. Golokhvast, Comparison of the Level and Mechanisms of Toxicity of Carbon Nanotubes , Carbon Nanofibers , and Silicon Nanotubes in Bioassay with Four Marine Microalgae, Nanomaterials. 10 (2020) 485. doi:10.3390/nano10030485.

[15]   X. Yuan, X. Zhang, L. Sun, Y. Wei, X. Wei, Cellular Toxicity and Immunological Effects of Carbon-based Nanomaterials, Part. Fibre Toxicol. 16 (2019) 18. doi:10.1186/s12989-019-0299-z.

[16]   O.M. Rodriguez-Narvaez, J.M. Peralta-Hernandez, A. Goonetilleke, E.R. Bandala, Treatment technologies for emerging contaminants in water: A review, Chem. Eng. J. 323 (2017) 361–380. doi:10.1016/j.cej.2017.04.106.

[17]   O.M. Rodriguez-Narvaez, J.M. Peralta-Hernandez, A. Goonetilleke, E.R. Bandala, Biochar-supported nanomaterials for environmental applications, J. Ind. Eng. Chem. 78 (2019) 21–33. doi:10.1016/j.jiec.2019.06.008.

[18]   T. Do Minh, J. Song, A. Deb, L. Cha, V. Srivastava, M. Sillanpää, Biochar based catalysts for the abatement of emerging pollutants : A review, Chem. Eng. J. 394 (2020) 124856. doi:10.1016/j.cej.2020.124856.

[19]   X. Tan, Y. Liu, G. Zeng, X. Wang, X. Hu, Y. Gu, Z. Yang, Application of biochar for the removal of pollutants from aqueous solutions, Chemosphere. 125 (2015) 70–85. doi:10.1016/j.chemosphere.2014.12.058.

[20]   S. Mortazavian, T. Jones-Lepp, J.H. Bae, D. Chun, E.R. Bandala, J. Moon, Heat-treated biochar impregnated with zero-valent iron nanoparticles for organic contaminants removal from aqueous phase: Material characterizations and kinetic studies, J. Ind. Eng. Chem. 76 (2019) 197–214. doi:10.1016/j.jiec.2019.03.041.

[21]   L. Kaufman, P.J. Russeeuw, Finding groups in data: An introduction to cluster analysis, John Wiley & Sons, Ltd, Hobroken, NJ, 2009.

[22]   M. Schonlau, The clustergram: A graph for visualizing hierarchical and nonhierarchical cluster analyses, Stata J. 2 (2002) 391–402.

[23]   L. Stanberry, R. Nandy, D. Cordes, Cluster analysis of fMRI data using dendrogram sharpening, Hum. Brain Mapp. 20 (2003) 201–219.

[24]   J.P. Brans, Y. De Smet, PROMETHEE methods: Multiple criteria decision analysis, Springer Berlin Heidelberg, 2016.

[25] G.A. Ayoko, K. Singh, S. Balerea, S. Kokot, Exploratory multivariate modeling and prediction of the physico-chemical properties of surface water and groundwater, J. Hydorlogy. 336 (2007) 115–124.

[26] S.E. Omran, M. Shorafa, A.A. Zolfaghari, The effect of biochar on severity of soil water repellency of crude oil-contaminated soil, Environ. Sci. Pollut. Res. 27 (2020) 6022–6032. doi:10.1007/s11356-019-07246-9.

[27] Q. Fang, B. Chen, Y. Lin, Y. Guan, Aromatic and Hydrophobic Surfaces of Wood-derived Biochar Enhance Perchlorate Adsorption via Hydrogen Bonding to Oxygen- containing Organic Groups, Environ. Sci. Technol. 48 (2014) 279–288. doi:10.1021/es403711y.

[28] S. Yi, B. Witt, P. Chiu, M. Guo, P. Imhof, The origin and reversible nature of poultry litter biochar hydrophobicity, J. Environ. Qual. 44 (2015) 963–971. doi:10.2134/jeq2014.09.0385.

[29] A.H. Fahmi, A.W. Samsuri, H. Jol, D. Singh, Bioavailability and leaching of Cd and Pb from contaminated soil amended with different sizes of biochar, R. Soc. Open Sci. 5 (2018). doi:10.1098/rsos.181328.

[30] X. Ju, M. Bowden, E.E. Brown, X. Zhang, An improved X-ray diffraction method for cellulose crystallinity measurement, Carbohydr. Polym. 123 (2015) 476–481. doi:10.1016/j.carbpol.2014.12.071.

[31] S. Yoo, S.S. Kelley, D.C. Tilotta, S. Park, Structural Characterization of Loblolly Pine Derived Biochar by X-ray Diffraction and Electron Energy Loss Spectroscopy, ACS Sustain. Chem. Eng. 6 (2018) 2621–2629. doi:10.1021/acssuschemeng.7b04119.

[32] R.R. Domingues, P.F. Trugilho, C.A. Silva, I.C.N.A. De Melo, L.C.A. Melo, Z.M. Magriotis, M.A. Sánchez-Monedero, Properties of biochar derived from wood and high-nutrient biomasses with the aim of agronomic and environmental benefits, PLoS One. 12 (2017) 1–20. doi:10.1371/journal.pone.0176884.

[33] M. Zhang, K. Guan, Y. Ji, G. Liu, W. Jin, N. Xu, Controllable ion transport by surface-charged graphene oxide membrane, Nat. Commun. 10 (2019) 1–8. doi:10.1038/s41467-019-09286-8.

[34] X. Chen, X. Tang, Y.N. Liang, J.W. Cheah, P. Hu, X. Hu, Controlled thermal functionalization for dispersion enhancement of multi-wall carbon nanotube in organic solvents, J. Mater. Sci. 51 (2016) 5625–5634. doi:10.1007/s10853-016-9864-0.

[35] S. Chandra, J. Bhattacharya, In fluence of temperature and duration of pyrolysis on the property heterogeneity of rice straw biochar and optimization of pyrolysis conditions for its application in soils, J. Clean. Prod. 215 (2019) 1123+1139. doi:10.1016/j.jclepro.2019.01.079.

[36] H. Bekhti, H. Bouchafaa, R. Melouki, A. Travert, Y. Boucheffa, Adsorption of CO2 over MgO-impregnated NaYzeolites and modeling study, Microporous Mesoporous Mater. 294 (2020) 109866. doi:10.1016/j.micromeso.2019.109866.

[37] N. Ayawei, A.N. Ebelegi, D. Wankasi, Modelling and Interpretation of Adsorption Isotherms, J. Chem. 2017 (2017) 3039817. doi:10.1155/2017/3039817.

[38] C. Jung, J. Oh, Y. Yoon, Removal of acetaminophen and naproxen by combined coagulation and adsorption using biochar : influence of combined sewer overflow components, Environ. Sci. Pollut. Res. 22 (2015) 10058–10069. doi:10.1007/s11356-015-4191-6.

[39] V. Bernal, L. Giraldo, J.C. Moreno-Piraján, Thermodynamic analysis of acetaminophen and salicylic acid adsorption onto granular activated carbon : Importance of chemical

surface and effect of ionic strength, Thermochim. Acta. 683 (2020) 178467. doi:10.1016/j.tca.2019.178467.

[40]   Y. Ho, A.E. Ofomaja, Pseudo-second-order model for lead ion sorption from aqueous solutions onto palm kernel fiber, J. Hazard. Mater. 129 (2006) 137–142. doi:10.1016/j.jhazmat.2005.08.020.

Supplementary Information

Table S1. Numerical values for interlayer spacing (t_{002}), layer coherence (t_{100}), and number of graphene layers in the different biochar materials.

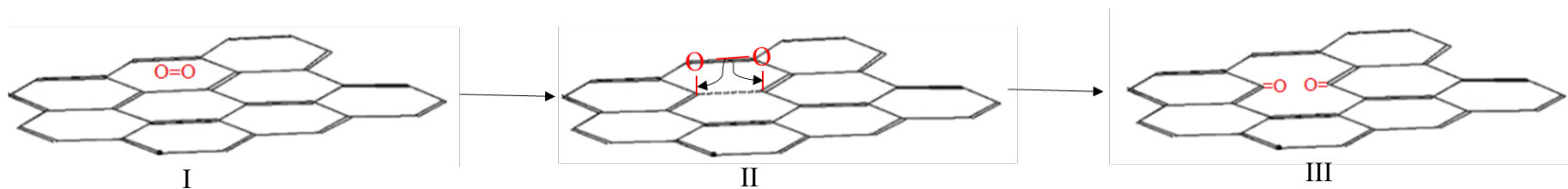| Biochar	t_{002}, nm	t_{100}, nm	# of graphene layer	Crystallinity Index, %
BC	1.42	1.25	4.26	82.5
3.5BC	0.95	0.90	3.4	79.4
8BC	1.14	1.69	2.85	79.5
24BC	1.35	1.20	3.05	83.3

Figure S1. Schematic mechanism proposed for oxygen-containing functional groups production in the graphene layers of biochar I) 1,2 peroxidation, II) homolytic breaking of C-C and O-O bonds, III) carboxyl groups generation.
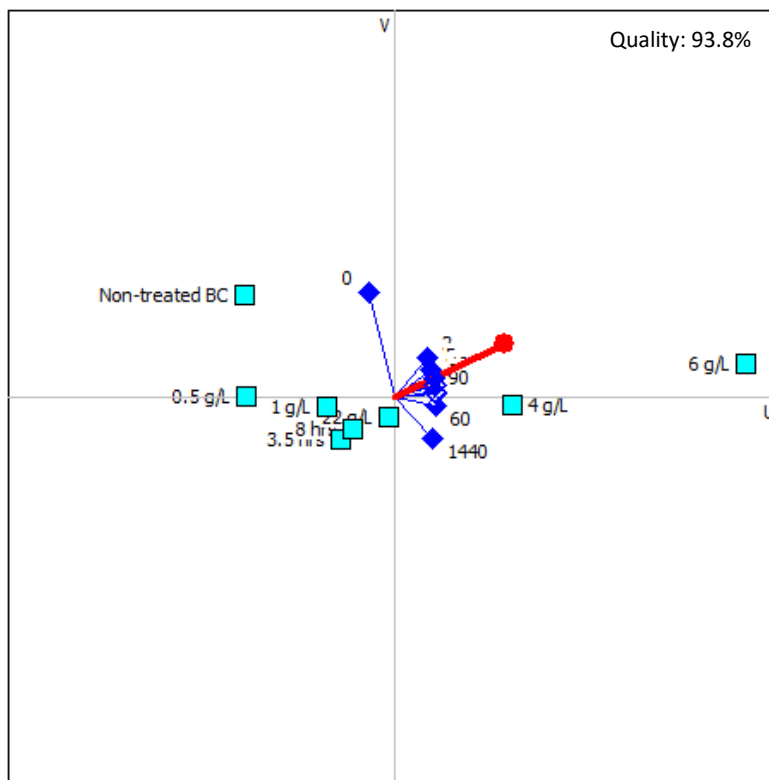
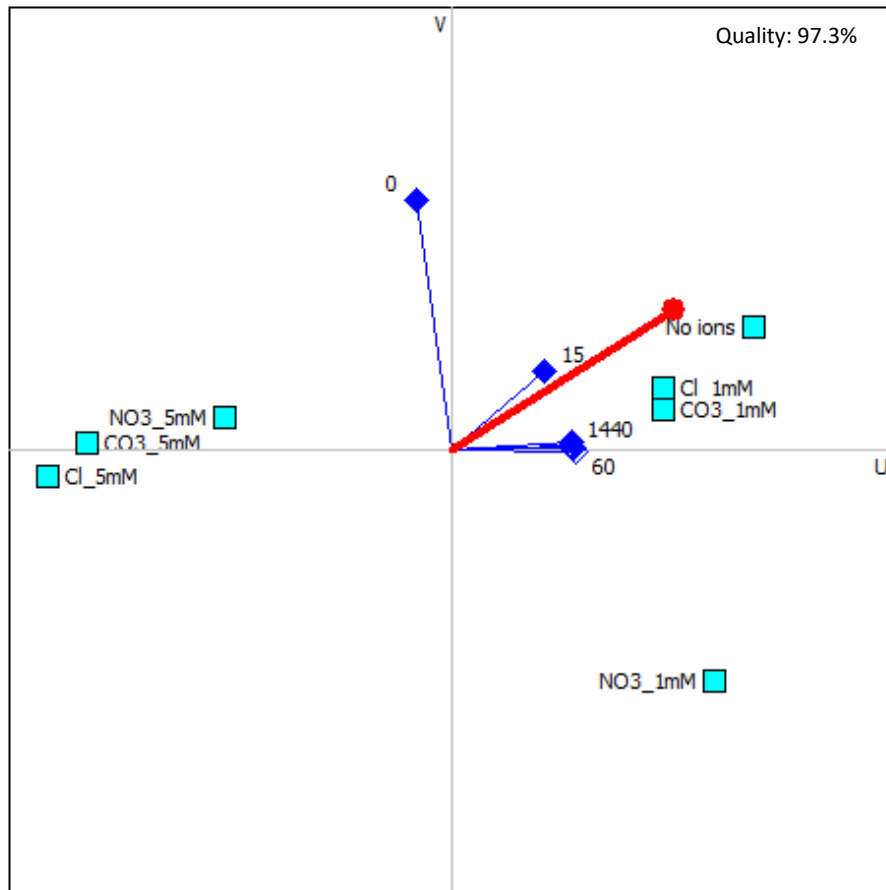Figure S2. GAIA biplot for ACT adsorption in different biochar materials.
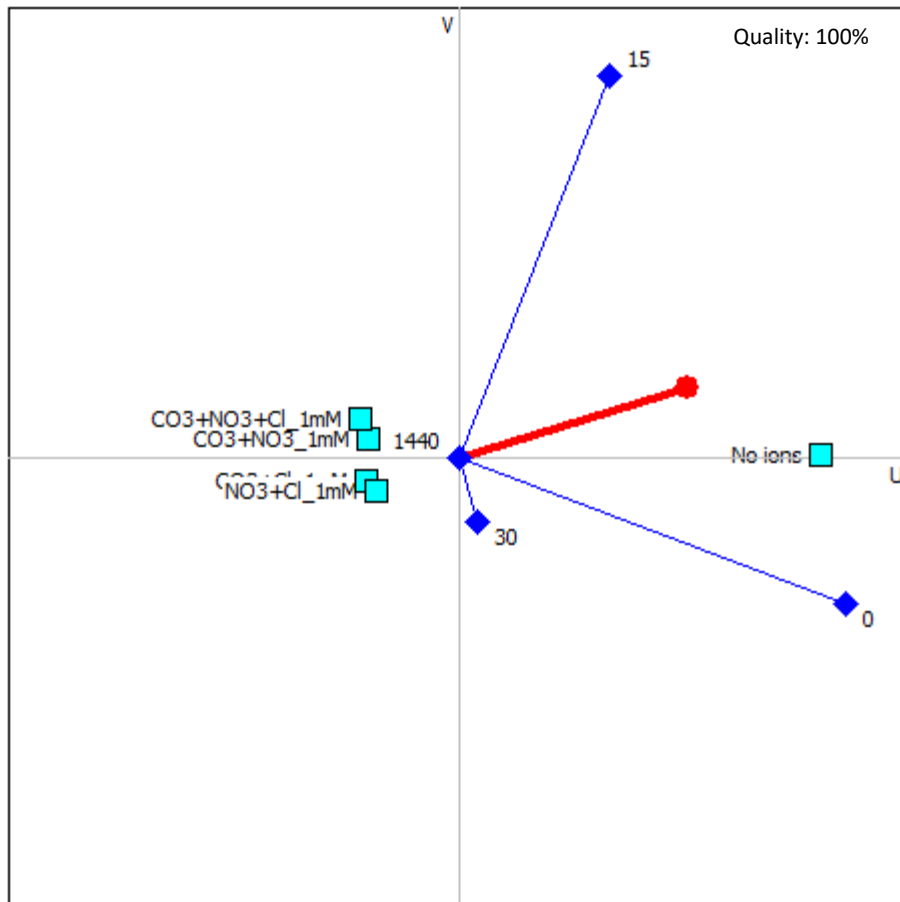
Figure S3. GAIA biplot for ACT adsorption in single ion system.

Figure S4. GAIA biplot for ACT adsorption in multiple ion system.